



Audio Engineering Society Convention Paper

Presented at the 138th Convention
2015 May 7–10 Warsaw, Poland

This paper was peer-reviewed as a complete manuscript for presentation at this Convention. Additional papers may be obtained by sending request and remittance to Audio Engineering Society, 60 East 42nd Street, New York, New York 10165-2520, USA; also see www.aes.org. All rights reserved. Reproduction of this paper, or any portion thereof, is not permitted without direct permission from the Journal of the Audio Engineering Society.

Physical Properties of Local Wave Field Synthesis using Linear Loudspeaker Arrays

Fiete Winter and Sascha Spors

Institute of Communications Engineering, University of Rostock, R.-Wagner-Str. 31 (H8), 18119 Rostock, Germany

Correspondence should be addressed to Fiete Winter (fiete.winter@uni-rostock.de)

ABSTRACT

Wave Field Synthesis aims at a physically accurate synthesis of a desired sound field inside an extended listening area. Due to limitation of practical loudspeaker setups, the accuracy of this sound field synthesis technique over the entire listening area is limited. Local Wave Field Synthesis narrows the spatial extent down to a local listening area in order to improve the reproduction accuracy inside this limited region. Recently an method has been published, which utilizes focused sources as a distribution of more densely placed virtual secondary sources around the local area. Within this paper, an analytical framework is established to analyze the physical properties of this approach for linear loudspeaker setups.

1. INTRODUCTION

Sound field synthesis (SFS) techniques synthesize a desired acoustic scenario within an extended listening area. Wave Field Synthesis (WFS) and Higher-Order Ambisonics (HOA) are two well known examples of these reproduction techniques. In theory, WFS creates a reproduction of a virtual wave field using a continuous distribution of acoustic sources. A limited number (up to hundreds) of individually driven loudspeakers placed at discrete positions around the listening area realizes this distribution in practical implementations. The finite spatial resolution of this discretization induces spatial aliasing artifacts to the reproduced wave field and therefore limits the synthesis accuracy. Current setups

for WFS do not allow for an accurate synthesis within the extended area for the full audible frequency range up to 20 kHz.

For application scenarios, where the listeners' position is further restricted to smaller region of interest, local sound field synthesis (LSFS) techniques are useful. They aim at a more accurate synthesis within a (local) area which is smaller than the entire area surrounded by the loudspeaker array. This accuracy improvement comes at the cost of stronger artifacts outside the local listening area. Among other approaches [1, 2, 3, 4] for LSFS, a technique [5] has been proposed which utilizes focused sources as virtual loudspeakers surrounding the local listening area. Analogue to conventional SFS these virtual

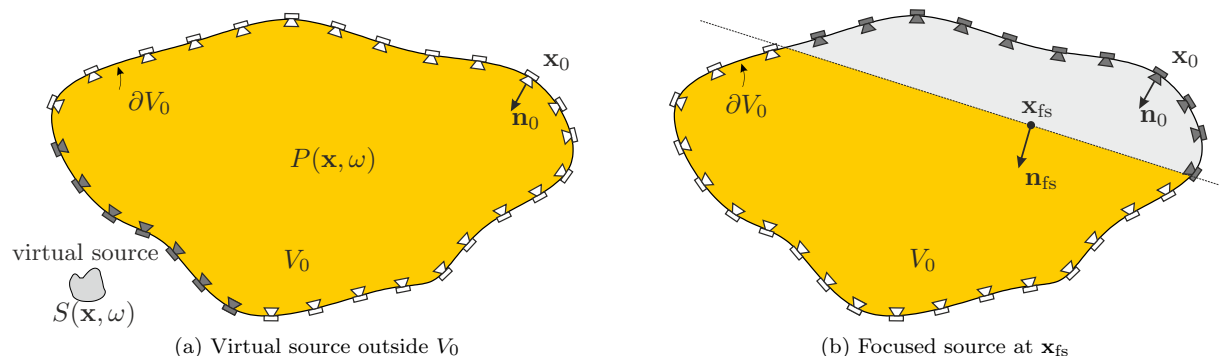


Fig. 1: The desired sound field is only reproduced correctly inside the listening area (yellow shade), which is a subset of V_0 for reproduction of focused sources (b). The active (dark shaded) loudspeakers for the scenarios (a) and (b) are selected via the secondary selection criteria $a(\mathbf{x}_0)$ and $a_{fs}(\mathbf{x}_0 - \mathbf{x}_{fs})$, respectively.

loudspeakers are driven by a suitable SFS technique in order to reproduce the desired wave field within the local listening area. The SFS driven focused sources are then realized by the real loudspeaker setup. It has been shown in [5], that Wave Field Synthesis is a computationally efficient tool for implementing this LSFS technique.

This paper analyzes the mentioned Local Wave Field Synthesis (LWFS) approach with respect to physical properties for linear loudspeaker arrays. It focuses on the artifacts introduced by spatial sampling and truncation of the real and the virtual loudspeaker distributions. First, a short overview on the basic theory of WFS and focused sources for arbitrary array geometries is given in Sec. 2. An analytical framework based on this theory is established for LWFS. Secondly, aliasing criteria for infinitely long arrays are derived by using spatio-spectral representations of the involved functions. Thirdly, the effects of array truncation in combination with spatial sampling are highlighted.

2. BASIC THEORY

2.1. Wave Field Synthesis

WFS is based on the Helmholtz Integral Equation (HIE) [6, 7], which states the solution of the homogeneous wave equation for a bounded region V_0 with respect to inhomogeneous boundary conditions imposed on ∂V_0 . A loudspeaker setup, which is placed on the boundary ∂V_0 , can be regarded as an inhomogeneous boundary condition.

For the application of sound field synthesis it is

desired to reproduce the sound field $S(\mathbf{x}, \omega)$ of a virtual source outside the listening area V_0 (see Fig. 1a). The HIE states that a distribution of secondary monopole and dipole sources on the boundary ∂V_0 has to be driven by the directional gradient and pressure of the sound field of the virtual source in order to achieve the sound field reproduction inside V_0 . In this case, the sound field $P(\mathbf{x}, \omega)$ inside the listening area coincides with the desired sound field $S(\mathbf{x}, \omega)$. While the theory of WFS states the exact solution of the HIE for infinite planar (3D) secondary source distributions, it introduces a number of reasonable approximations to circumvent the necessity of secondary dipole sources for arbitrarily shaped boundaries. The synthesized sound field is given by

$$P(\mathbf{x}, \omega) = - \oint_{\partial V_0} D(\mathbf{x}_0, \omega) G_0(\mathbf{x} - \mathbf{x}_0, \omega) dA_0, \quad (1)$$

where a position on the boundary ∂V_0 is denoted by $\mathbf{x}_0 \in \partial V_0$. The free-field Green's function $G_0(\mathbf{x} - \mathbf{x}_0, \omega)$ characterizes the sound field emitted by a secondary spherical monopole source located at \mathbf{x}_0 . $D(\mathbf{x}_0, \omega)$ describes the driving function for the secondary sources and dA_0 a suitably chosen boundary element for integration. The WFS driving function for the secondary sources is given as

$$D(\mathbf{x}_0, \omega) = 2a(\mathbf{x}_0) \frac{\partial}{\partial \mathbf{n}_0} S(\mathbf{x}, \omega), \quad (2)$$

where the directional gradient $\frac{\partial}{\partial \mathbf{n}_0}$ is defined as scalar product of the boundary's inward normal vector \mathbf{n}_0 and the gradient $\nabla S(\mathbf{x}, \omega)$ evaluated at

$\mathbf{x} = \mathbf{x}_0$.

The secondary source selection criterion $a(\mathbf{x}_0)$ ensures that only those secondary sources are active where the propagation direction of virtual source $S(\mathbf{x}, \omega)$ at the position \mathbf{x}_0 has a positive component in direction of the normal vector \mathbf{n}_0 .

2.2. Focused Sources

Amongst other sound field synthesis techniques, WFS allows for the synthesis of so called *focused sources*. They aim at creating the impression of a monopole source, which is placed in front of the loudspeaker array. This can be achieved by emitting a sound field which converges towards a *focus point* $\mathbf{x}_{fs} \in V_0$ and diverges after (see Fig. 1b). The underlying principle is termed acoustic focusing by time reversal/phase conjugation [8, 9, 10].

In order to avoid listener's confusion caused by converging contributions, only those emerging from the desired focused source should be reproduced at the listener position. The secondary sources emit a sound field that travels towards the listener. It can therefore be expected, that the desired sound field of a focused source is only correct if the focus point is located between the active secondary sources and the listening position. This is a well known limitation of WFS in the context of synthesized focused sources [11].

The driving function for a focused source can be derived by considering a virtual monopole sink which is characterized by the time-reversed (complex conjugated) free field Green's function $G_0^*(\mathbf{x} - \mathbf{x}_{fs}, \omega)$. Additionally, a reasonable selection of the active secondary sources ensures causality in practice. The driving function is given as

$$D_{fs}(\mathbf{x}_0 - \mathbf{x}_{fs}, \omega) = -2 a_{fs}(\mathbf{x}_0 - \mathbf{x}_{fs}) \frac{\partial}{\partial \mathbf{n}_0} G_0^*(\mathbf{x} - \mathbf{x}_{fs}, \omega), \quad (3)$$

where the secondary source selection criteria

$$a_{fs}(\mathbf{x}_0 - \mathbf{x}_{fs}) = \begin{cases} 1 & , \text{ if } \mathbf{n}_{fs}^T(\mathbf{x}_0 - \mathbf{x}_{fs}) < 0 \\ 0 & , \text{ otherwise} \end{cases} \quad (4)$$

ensures that only secondary sources which contribute to the main propagation direction \mathbf{n}_{fs} are active. The listening area of a focused source is limited by a plane through the focus point \mathbf{x}_{fs} (see Fig. 1b). The plane's normal is defined by the orientation \mathbf{n}_{fs}

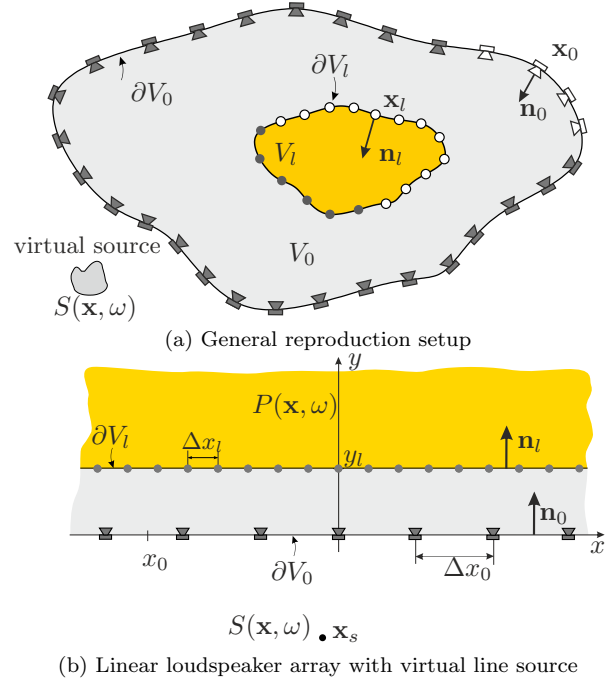


Fig. 2: In Local Wave Field Synthesis the desired sound field $S(\mathbf{x}, \omega)$ is only reproduced correctly inside the local listening area V_l (yellow shade) with the virtual secondary source distribution (dots) on its boundary ∂V_l . Active (virtual) secondary sources are shaded dark.

of the focused source. Hence, the reproduced sound field

$$P(\mathbf{x}, \omega) = - \oint_{\partial V_0} D_{fs}(\mathbf{x}_0 - \mathbf{x}_{fs}, \omega) G_0(\mathbf{x} - \mathbf{x}_0, \omega) dA_0 \quad (5)$$

approximates the desired sound field $S(\mathbf{x}, \omega) = G_0(\mathbf{x} - \mathbf{x}_{fs}, \omega)$ of a focused point source only for listening positions $\mathbf{x} \in V_0$ where $\mathbf{n}_{fs}^T(\mathbf{x} - \mathbf{x}_{fs}) > 0$ is fulfilled.

Although the wave field of a monopole source consists of propagating and evanescent contributions, time-reversal focusing cannot reproduce its evanescent part correctly [10, 9]. This limitation is due to the reciprocity theorem of Shewell and Wolf [12, (4.11-4.14)], which only holds for propagating wave fields. The correct reproduction of evanescent wave field components is therefore not considered in this paper.

2.3. Local Wave Field Synthesis

The basic concept of LWFS is to utilize a set of focused sources as a so called *virtual secondary source* distribution, which has to be driven like a real loudspeaker setup. The virtual secondary sources are distributed on the boundary ∂V_l of the local listening area $V_l \subset V_0$ (see Fig. 2a). The driving signal for the virtual secondary sources is derived by migrating the equations (1) and (2) of the WFS approach (see Sec. 2.1) to the geometry of the local listening area. This domain denoted by the index "l" is referred to the *local domain*, while the *loudspeaker domain* (index 0) describes the physically existing secondary source geometry. The driving signal then reads

$$D_l(\mathbf{x}_l, \omega) = 2 a_l(\mathbf{x}_l) \frac{\partial}{\partial \mathbf{n}_l} S(\mathbf{x}, \omega), \quad (6)$$

while the reproduced local sound field is given as

$$P(\mathbf{x}, \omega) = - \oint_{\partial V_l} D_l(\mathbf{x}_l, \omega) G_0(\mathbf{x} - \mathbf{x}_l, \omega) dA_l \quad (7)$$

for $\mathbf{x} \in \partial V_l$. The free field Green's function $G_0(\mathbf{x} - \mathbf{x}_l, \omega)$ is realized by a focused point source. Its propagating part can be correctly reproduced inside V_l by the means of equation (5), assuming a convex boundary ∂V_l . $G_0(\mathbf{x} - \mathbf{x}_l, \omega)$ is therefore replaced by the right-hand side of (5) with $\mathbf{x}_{fs} = \mathbf{x}_l$. After a rearrangement of the integrals' order the reproduced sound field is expressed by

$$P(\mathbf{x}, \omega) = - \oint_{\partial V_0} D_0(\mathbf{x}_0, \omega) G_0(\mathbf{x} - \mathbf{x}_0, \omega) dA_0, \quad (8)$$

while the LWFS driving function for the secondary sources is given as

$$D_0(\mathbf{x}_0, \omega) = - \oint_{\partial V_l} D_l(\mathbf{x}_l, \omega) D_{fs}(\mathbf{x}_0 - \mathbf{x}_l, \omega) dA_l. \quad (9)$$

3. INFINITE LINEAR LOUDSPEAKER ARRAY

Typical implementations of WFS systems are restricted to the reproduction in the horizontal plane only using (piecewise) linear loudspeaker arrays [5]. Modeling each loudspeaker as a monopole point source is referred to as 2.5D WFS. The following calculus is however simplified to a two-dimensional scenario utilizing secondary line sources. The effects of spatial aliasing and truncation on 2.5D setups can

Spatial Fourier Transform along the x -axis

$$\tilde{F}(k_x, y, \omega) = \int_{-\infty}^{\infty} F(\mathbf{x}, \omega) e^{jk_x x} dx$$

$$\tilde{D}_l(k_x, \omega) = -e^{jk_x x_s} \begin{cases} e^{j\sqrt{(\frac{\omega}{c})^2 - k_x^2} (y_s - y_l)} \\ e^{\sqrt{k_x^2 - (\frac{\omega}{c})^2} (y_s - y_l)} \end{cases}$$

$$\tilde{D}_{fs}(k_x, \omega) = \begin{cases} -e^{j\sqrt{(\frac{\omega}{c})^2 - k_x^2} y_l} \\ -e^{-\sqrt{k_x^2 - (\frac{\omega}{c})^2} y_l} \end{cases}$$

$$\tilde{G}_0(k_x, y, \omega) = \begin{cases} -\frac{j}{2} \frac{e^{-j\sqrt{(\frac{\omega}{c})^2 - k_x^2} y}}{\sqrt{(\frac{\omega}{c})^2 - k_x^2}} \\ 1 \frac{e^{-\sqrt{k_x^2 - (\frac{\omega}{c})^2} y}}{2 \sqrt{k_x^2 - (\frac{\omega}{c})^2}} \end{cases}$$

Table 1: Spatial Fourier spectra of driving signals $D_l(\mathbf{x}_l, \omega)$ [13, (9)], $D_{fs}(\mathbf{x}_0 - \mathbf{x}_l, \omega)$ [14, (10)] and free field Green's function $G_0(\mathbf{x} - \mathbf{x}_0, \omega)$ [13, (8)] for the reproduction scenario illustrated in Fig. 2b.

be inferred from the 2D case [13, 14]. The theoretical basis for linear secondary line source distributions is given by Rayleigh's first integral equation. The integral states that a linear distribution of monopole line sources is capable of reproducing a desired wave in one of the half planes defined by the linear distribution.

An exemplary situation is illustrated in Fig. 2b: The linear loudspeaker array is located on the x -axis ($y = 0$) while the virtual secondary distribution is placed parallel to the loudspeakers ($y = y_l$). For the given geometry of this scenario the normal vectors $\mathbf{n}_0 = \mathbf{n}_l = [0 \ 1]^T$. The reproduced wave field is given by the Rayleigh I integral

$$P(\mathbf{x}, \omega) = - \int_{-\infty}^{\infty} D_0(\mathbf{x}_0, \omega) G_0(\mathbf{x} - \mathbf{x}_0, \omega) dx_0, \quad (10)$$

where $\mathbf{x} = [x \ y]^T$ with $y > 0$ and $\mathbf{x}_0 = [x_0 \ 0]^T$. The two-dimensional free-field Green's function [6]

$$G_0(\mathbf{x} - \mathbf{x}_0, \omega) = -\frac{j}{4} H_0^{(2)}\left(\frac{\omega}{c} |\mathbf{x} - \mathbf{x}_0|\right) \quad (11)$$

describes the wave field of the loudspeakers for two-dimensional reproduction. The Hankel function of second kind and zeroth-order is denoted by $H_0^{(2)}(\cdot)$.

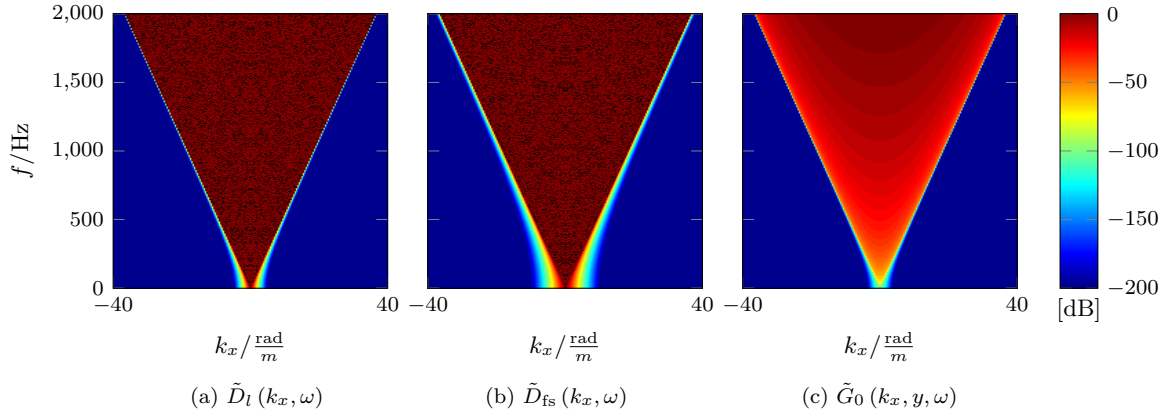


Fig. 3: Absolute values of spatial spectra shown in Tab. 1. The virtual source position $\mathbf{x}_s = [x_s \ y_s]^T = [0 \ -1]^T$ m, while $y_l = 1$ m and $y = 2$ m. The propagating part ($|k_x| < |\frac{\omega}{c}|$) of the respective spectra can be recognized by the red triangle, while the evanescent contributions rapidly decay towards zero for $|k_x| > |\frac{\omega}{c}|$.

The secondary sources' driving function is given by the spatial convolution integral

$$D_0(\mathbf{x}_0, \omega) = - \int_{-\infty}^{\infty} D_l(\mathbf{x}_l, \omega) D_{fs}(\mathbf{x}_0 - \mathbf{x}_l, \omega) dx_l, \quad (12)$$

where $\mathbf{x}_l = [x_l \ y_l]^T$ with $y_l > y_0$. In this paper we investigate physical properties of LWFS with respect to a virtual line source as the desired sound field. This source type poses the two-dimensional analogon to the monopole point source in a three-dimensional scenario. The wave field of the virtual source is therefore given by the wave field of a monopole line source

$$S(\mathbf{x}, \omega) = -\frac{j}{4} H_0^{(2)}\left(\frac{\omega}{c} |\mathbf{x} - \mathbf{x}_s|\right), \quad (13)$$

where $\mathbf{x}_s = [x_s \ y_s]^T$ defines the position of the source with $y_s < 0$.

3.1. Spatio-temporal Frequency Representation

The reproduced sound field is given, accordingly to eq. (10) and (12), as two convolutions along the x -axis. This is illustrated by a block diagram (Fig. 4). Applying a spatial Fourier transformation to both equations with respect to the x -coordinate yields

$$\tilde{P}(k_x, y, \omega) = \underbrace{\tilde{D}_l(k_x, \omega) \tilde{D}_{fs}(k_x, \omega)}_{-\tilde{D}_0(k_x, \omega)} \tilde{G}_0(k_x, y, \omega). \quad (14)$$

The three spectra on the equation's right-hand side are shown in Tab. 1 and their absolute values are

plotted in Fig. 3. The secondary sources' driving signal is given by combining the spatial spectra of the two driving signals of eq. (14) to

$$\tilde{D}_0(k_x, \omega) = -e^{jk_x x_s} \times \begin{cases} e^{j\sqrt{(\frac{\omega}{c})^2 - k_x^2} y_s} & \text{for } |k_x| < |\frac{\omega}{c}|, \\ e^{\sqrt{k_x^2 - (\frac{\omega}{c})^2} (y_s - 2y_l)} & \text{for } |\frac{\omega}{c}| < |k_x|. \end{cases} \quad (15)$$

Interestingly, the propagating contribution of the driving signal equals the traditional WFS driving signal [13, (9)] for a virtual line source reproduced by a linear secondary source distribution. This can be explained by comparing the Rayleigh I integral (10) with regard to both secondary source distributions at ∂V_l and ∂V_0 : As long the virtual source is located outside V_0 ($y_s < 0$) the propagating part of the virtual source's wave field will be reproduced correctly for $\mathbf{x} \in V_l$ using either of the distributions driven by the respective WFS driving signals. As already mentioned in Sec. 2.2, the evanescent part is not reproduced correctly.

3.2. Spatial Sampling

It has already been outlined by Start [15, p. 73-79] that the discretization of the (virtual) secondary source distribution can be interpreted as a spatial sampling and interpolation process. As illustrated in Fig. 4, this process is divided into two sub-steps for the local and the loudspeaker domain, both applying sampling and interpolation. The spatial sampling is

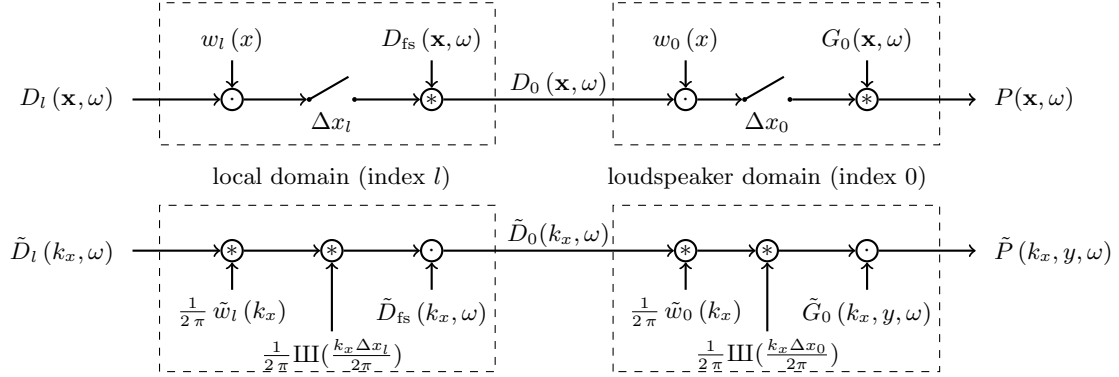


Fig. 4: The upper part of the block diagram illustrates the eqs. (10) and (12). The effects of spatial sampling ($\Delta x_l, \Delta x_0$) are highlighted in Sec. 3.2. The spatial window functions $w_l(x)$ and $w_0(x)$ cover the truncation effects explained in Sec. 4. The spatial Fourier transform of each system component with respect to the x -coordinate is depicted in the lower part of the figure.

modeled by multiplying the respective driving signal with a Dirac comb

$$\text{III}_{\{0,l\}}(x) = \frac{1}{\Delta x_{\{0,l\}}} \sum_{\mu=-\infty}^{\infty} \delta(x - \mu \Delta x_{\{0,l\}}) \quad (16)$$

with the sampling distance $\Delta x_{\{0,l\}}$. The wildcard symbol $\{0,l\}$ is replaced by either 0 or l for the respective domain. The spatial k_x -spectra of the discretized driving signals

$$\tilde{D}_{\{0,l\}}^S(k_x, \omega) = 2\pi \sum_{\mu=-\infty}^{\infty} \tilde{D}_{\{0,l\}} \left(k_x - \mu \frac{2\pi}{\Delta x_{\{0,l\}}}, \omega \right) \quad (17)$$

are given as a superposition of the shifted continuous spectra $\tilde{D}_{\{0,l\}} \left(k_x - \mu \frac{2\pi}{\Delta x_{\{0,l\}}}, \omega \right)$. After each sampling step the spatial interpolation filters $\tilde{D}_{fs}(k_x, \omega)$ and $\tilde{G}_0(k_x, y, \omega)$ are applied, respectively. Introducing the sampled driving functions $\tilde{D}_l^S(k_x, \omega)$ and $\tilde{D}_0^S(k_x, \omega)$ into eq. (14) results in the spectrum $\tilde{P}^S(k_x, y, \omega)$ of the wave field reproduced by a spatially discrete (virtual) secondary source distribution. It is worth noting, that this equation (14) is not commutative due to the spatial sampling. Figure 5 illustrates the calculation for each domain on a qualitative level. The gray triangles symbolize the propagating part of the involved continuous spectra. The spectral repetitions of the discretized driving functions are shaded red and blue, respectively. Aliasing contributions can be recognized by

the overlapping parts of the continuous spectra and the spectral repetitions. Due to the concatenation of both calculation steps (Fig. 5a and 5b), the resulting wave field $\tilde{P}^S(k_x, y, \omega)$ might contain aliasing contributions from both steps. For the reproduced sound field the anti-aliasing condition of [13, 14, 16] is therefore extended to

$$f_{al} \leq \min \left(\frac{c}{2\Delta x_l}, \frac{c}{2\Delta x_0} \right), \quad (18)$$

where c denotes the speed of sound. The anti-aliasing frequency f_{al} can not be increased by additional virtual secondary sources (smaller Δx_l), since the distance between the loudspeakers (Δx_0) remains as the limiting factor in practical setups. For an infinite linear loudspeaker distribution LWFS does not lead to a benefit in terms of aliasing compared to the traditional WFS method in [13, (13)].

4. FINITE LINEAR LOUDSPEAKER ARRAY

For practical reproduction setups linear loudspeaker arrays are of finite length. Also the number of virtual secondary sources has to be finite due to limited computational resources. Both truncations are modelled by multiplying the respective driving function $\tilde{D}_{\{0,l\}}(\mathbf{x}_{\{0,l\}}, \omega)$ with a suitable window $w_{\{0,l\}}(x_{\{0,l\}})$ (see Fig. 4). Again, the wildcard character $\{0,l\}$ denotes either 0 or l for the respective domain. In this paper, the rectangular window

function

$$w_{\{0,l\}}(x_{\{0,l\}}) = \text{rect}\left(\frac{x_{\{0,l\}} - X_{\{0,l\}}}{L_{\{0,l\}}}\right) \quad (19)$$

is chosen to model distributions of finite length $L_{\{0,l\}}$ centered around $X_{\{0,l\}}$. The shifted rect-function [17, p. 201-204] equals unity for $|x_{\{0,l\}} - X_{\{0,l\}}| \leq L_{\{0,l\}}/2$ and zero otherwise. The spatial spectra of the driving function

$$\tilde{D}_{\{0,l\}}^{\text{tr}}(k_x, \omega) = \frac{1}{2\pi} \tilde{w}_{\{0,l\}}(k_x) * \tilde{D}_{\{0,l\}}(k_x, \omega) \quad (20)$$

is derived using the multiplication theorem of the Fourier transform. The spatial Fourier transform of $w_{\{0,l\}}(x_{\{0,l\}})$ is given as

$$\tilde{w}_{\{0,l\}}(k_x) = L_{\{0,l\}} \text{sinc}\left(\frac{k_x}{2} L_{\{0,l\}}\right) e^{jk_x X_{\{0,l\}}}, \quad (21)$$

while $\text{sinc}(x) := \sin(x)/x$. It is worth noting, that the truncated driving function $\tilde{D}_0^{\text{tr}}(\mathbf{x}_0, \omega)$ depends on both window functions due to the concatenation of the local and loudspeaker domain (see Fig. 4).

Figure 6a shows the effects of a truncated virtual secondary source distribution on $D_l(k_x, \omega)$: As already discussed in [13], the energy of the truncated driving function $\tilde{D}_l^{\text{tr}}(k_x, \omega)$ is concentrated in a smaller region compared to the infinite length distribution (see Fig. 3a). This energy concentration has influence on the spatial aliasing properties of the spectra. The same effect can be observed for the loudspeaker's driving function $\tilde{D}_0^{\text{tr}}(k_x, \omega)$ (see Fig. 6b and 6c). Note that in Fig. 6b no truncation in the local domain is applied because of the infinite length L_l . In order to investigate the connection between these three spectra a geometric approximation is applied. It is furthermore used to derive an anti-aliasing criterion for local wave field synthesis with finite linear loudspeaker arrays.

4.1. Geometric Approximation

The limited listening area as a result of the truncation can be approximated by geometric means for a given position of the virtual line source [13]. This approach is further extended to analyze the truncation effects of the local and loudspeaker domain. For each domain a wedge shaped area is spanned by the virtual position and the endings of the respective secondary source distribution (see Fig. 7a). The angles $\alpha_{\{0,l\}}$ and $\beta_{\{0,l\}}$ between the sides of each wedge

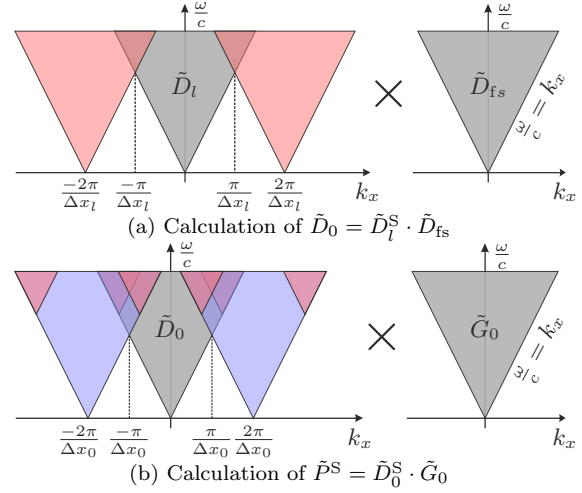


Fig. 5: Qualitative illustration of the two sampling and interpolation processes involved in the computation of the propagating parts of reproduced wave field $\tilde{P}^S(k_x, y, \omega)$ for a sampled (virtual) secondary source distribution.

to the x -axis are given as

$$\tan \alpha_{\{0,l\}} = \frac{y_{\{0,l\}} - y_s}{X_{\{0,l\}} + \frac{L_{\{0,l\}}}{2} - x_s}, \quad (22a)$$

$$\tan \beta_{\{0,l\}} = \frac{y_{\{0,l\}} - y_s}{X_{\{0,l\}} - \frac{L_{\{0,l\}}}{2} - x_s}, \quad (22b)$$

where $0 \leq \alpha_{\{0,l\}}, \beta_{\{0,l\}} \leq \pi$ and $\alpha_{\{0,l\}} \leq \beta_{\{0,l\}}$. The length L_0 and the center position X_0 of the secondary source distribution are fixed because a practical loudspeaker setup remains static. Therefore, the angles α_0 and β_0 define a fixed outer bound of the listening area for a given virtual source position \mathbf{x}_s . The listening area is further constrained by the parameters X_l and L_l , which may be set with respect to the listeners' position and the position of the virtual line source. Since both domains are concatenated the intersection of the wedge shaped areas yields the final listening area. Its boundary is defined by the angles

$$\alpha_B = \max(\alpha_0, \alpha_l) \quad \text{and} \quad (23a)$$

$$\beta_B = \min(\beta_0, \beta_l), \quad (23b)$$

where $\alpha_0 \leq \beta_l$ and $\alpha_l \leq \beta_0$ holds. If this condition is not fulfilled the wedges are disjoint and no listening area is established. Hence the virtual line source is

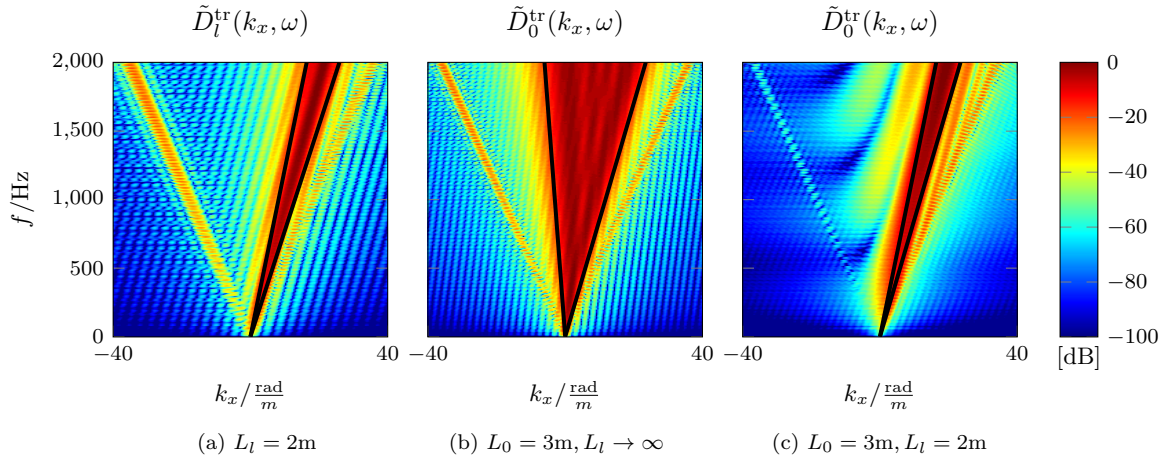


Fig. 6: Magnitude spectra of truncated driving functions. The virtual source position $\mathbf{x}_s = [x_s \ y_s]^T = [-1, -3]^T \text{m}$, while the center of the virtual secondary source distribution is located at $[X_l, y_l]^T = [1, 2]^T \text{m}$. The loudspeaker array is centered around $[X_0, y_0]^T = \mathbf{0}$.

not reproduced for any listener position. Vice versa the set of possible virtual source positions is limited for a given array geometry by the angles $\gamma_1 \leq \alpha_B$ and $\gamma_2 \geq \beta_B$ (see Fig. 7b) given as

$$\tan \gamma_1 = \frac{y_l - y_0}{\left(X_l + \frac{L_l}{2}\right) - \left(X_0 - \frac{L_0}{2}\right)}, \quad (24a)$$

$$\tan \gamma_2 = \frac{y_l - y_0}{\left(X_l - \frac{L_l}{2}\right) - \left(X_0 + \frac{L_0}{2}\right)}. \quad (24b)$$

In order to bring the geometric approximation in conjunction with the effect of truncation on the driving functions, their spatial spectra $D_{\{0,l\}}^{\text{tr}}(k_x, \omega)$ are re-interpreted as a superposition of plane wave contributions (termed as *plane wave decomposition*) [13]. These contributions are derived by substituting k_x with

$$k_x = \frac{\omega}{c} \cos \phi \quad (25)$$

where ϕ denotes the plane wave's incidence angle. For a more detailed description the reader is referred to [13]. The geometric approximation essentially states that the major plane wave contributions will be limited within the incidence angles α_B and β_B . These limits are shown in Fig. 6c by the black lines. α_l, β_l and α_0, β_0 are respectively depicted in Fig. 6a and Fig. 6b in order to show the impact of both truncations on the spectra. For all three spectra the geometric approximation states a reasonable instrument to describe the energy concentration imposed

by the truncation of the driving functions.

The angles γ_1 and γ_2 were specified in eq. (24) as limits for the reproducible virtual source position. They also state outer bounds for plane wave contributions which can be reproduced by a given array geometry. This is of interest when defining anti-aliasing criteria for discrete secondary source distributions.

4.2. Anti-Aliasing Conditions

In the following anti-aliasing conditions for discrete and truncated (virtual) secondary source distribution are derived using the geometric approximation for truncated driving functions.

First, the effects of a discrete virtual secondary source distribution with a sampling distance of Δx_l are investigated. Analogue to Sec. 3.2, spatial sampling induces spectral repetitions of the continuous, truncated spectra $D_l^{\text{tr}}(k_x, \omega)$. The geometrically approximated spectra and its repetitions are depicted in Fig. 8a. It was mentioned at the end of section 4.1 that the reproducible plane wave contributions are limited within the angles γ_1 and γ_2 (green triangle) due to the concatenation of the two truncated arrays. Hence, only parts of the spectral repetitions overlapping with the reproducible spectra will contribute to aliasing. This happens if the temporal frequency $f \geq \min(f_{l,1}^{\text{al}}, f_{l,2}^{\text{al}})$ with the two aliasing

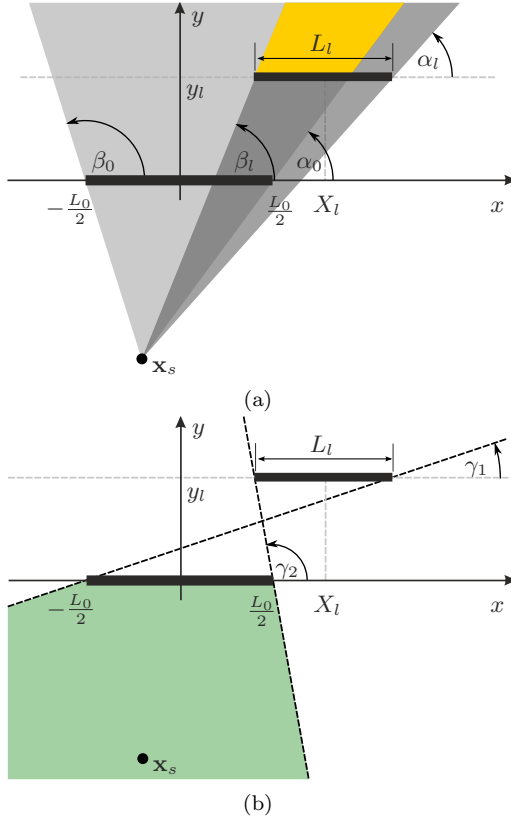


Fig. 7: The geometric approximation of listening area (yellow) in LWFS for a given virtual line source position is depicted in (a). The set of possible virtual line source positions (green) for a given array geometry is shown in (b).

frequencies

$$f_{l,1}^{\text{al}} = \frac{c}{\Delta x_l (\cos \alpha_l - \cos \gamma_2)}, \quad (26a)$$

$$f_{l,2}^{\text{al}} = \frac{c}{\Delta x_l (\cos \gamma_1 - \cos \beta_l)}. \quad (26b)$$

Since the virtual secondary source distribution of the local domain consists of synthesized focused sources, the sampling distance Δx_l is not constrained by the practical loudspeaker setup. The anti-aliasing frequencies can therefore be raised by realizing more focused sources, which is a matter of computational effort.

The discrete loudspeaker setup with a loudspeaker distance of Δx_0 analogously causes spectral repetitions of the continuous, truncated driving function

$D_0^{\text{tr}}(k_x, \omega)$. The sampled spectra is shown in Fig. 8b. The illustration assumes that no aliasing contributions from the local domain occur within the considered temporal frequency range ($\Delta x_l \ll \Delta x_0$). For listener's positions within the listening area defined by α_B and β_B (see Fig. 7a) aliasing effects for frequencies higher than

$$f_0^{\text{al}} = \frac{c}{\Delta x_0 (\cos \alpha_B - \cos \beta_B)}. \quad (27)$$

In comparison to eq. (26), this criterion is the more restrictive anti-aliasing condition since the sampling distance Δx_0 is connected to the physical reproduction setup, while Δx_l is only limited due to computational complexity.

4.3. Example

In the following an application example for the derived anti-aliasing conditions for truncated and sampled (virtual) secondary source distribution is given. A monochromatic ($f = 3000\text{Hz}$) line source placed at $\mathbf{x}_s = [0 \ -1]^T \text{m}$ is reproduced by a loudspeaker array consisting of 16 line sources with a spacing $\Delta x_0 = 0.20\text{m}$. The resulting array length is $L_0 = 3\text{m}$. The array is centered around $[X_0 \ y_0]^T = \mathbf{0}\text{m}$. The virtual secondary source distribution is defined by $L_l = 1\text{m}$ and $[X_l \ y_l]^T = [0 \ 1.5]^T \text{m}$. The angles limiting the local listening area can be derived from (22) and (23) as $\alpha_B \approx 78.7^\circ$ and $\beta_B \approx 101.3^\circ$. Inserting these angles and the sampling distance Δx_0 into (27) yields the aliasing frequency of $f_0^{\text{al}} \approx 4372\text{Hz}$. The speed of sound c is set to $343 \frac{\text{m}}{\text{s}}$ for this purpose.

Figure 9 shows the reproduction of the desired sound field with a traditional WFS and two LWFS setups. The latter differ in their sampling distance Δx_l of the virtual secondary source distribution. The second anti-aliasing frequency $f_l^{\text{al}} = f_{l,1}^{\text{al}} = f_{l,2}^{\text{al}}$ is derived from (24) and (26) for the two LWFS setups respectively yielding $f_l^{\text{al}} \approx 2066\text{Hz}$ and $f_l^{\text{al}} \approx 5509\text{Hz}$. Dominant aliasing artifacts can be observed for the first two reproduction setups (Fig. 9a and Fig. 9b). The more densely sampled virtual secondary source distribution depicted in Fig. 9c leads to more accurate reproduction of the desired sound field inside the local listening area. However, truncation artifacts (white stripes) are clearly visible near the edges of the local listening area. This is due to the fact, that the geometric derivation of the listening area's limits is a high frequency approximation.

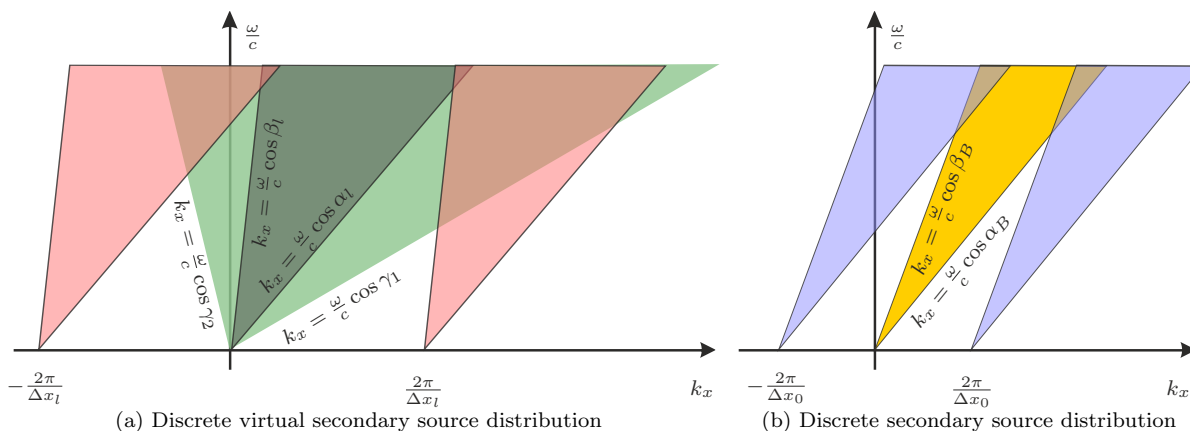


Fig. 8: Qualitative illustration of the aliasing contributions introduced in the local and in the loudspeaker domain

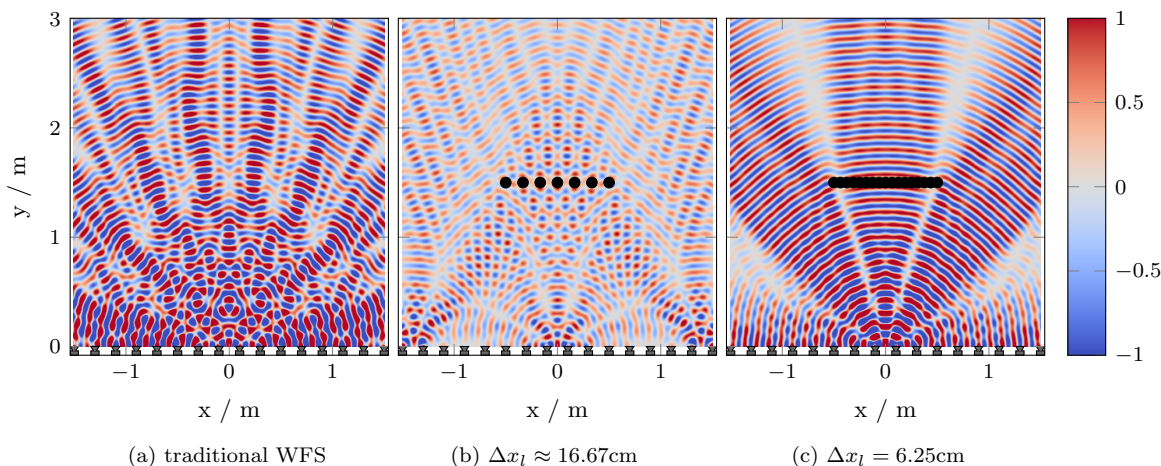


Fig. 9: The diagrams show the real part of the reproduced sound field for three different setups. The sound fields have been normalized to their respective absolute value at $[0 \ 2]^T$ m. While each loudspeaker is indicated by a symbol at the bottom of each plot, black dots represent the virtual secondary sources. The plots have been generated with the Sound Field Synthesis Toolbox [18].

5. CONCLUSION

This paper presented a detailed analysis of the physical properties of two-dimensional Local Wave Field Synthesis using focused line sources as virtual secondary sources. Anti-aliasing conditions have been derived for infinitely long and truncated linear secondary line source distributions. These state a trade-off between an artifact-free reproduction up to a certain temporal frequency and the size of the listening area for which the reproduction can be achieved. In principle, the derived anti-aliasing conditions will also hold for the more practical case of

2.5D reproduction using secondary point sources.

Listening experiments [19] have indicated that timbral perception of WFS is connected to spatial aliasing caused by the limited number of loudspeakers. Although the results of this paper might allow for the conclusion that the LWFS approach has better coloration properties than traditional WFS, subjective experiments have to be made in order to give a well-grounded judgment for this.

ACKNOWLEDGEMENTS

This research has been supported by EU FET grant TWO!EARS, ICT-618075.

6. REFERENCES

- [1] E. Corteel, C. Kuhn-Rahloff, and R. Pellegrini, "Wave Field Synthesis Rendering with Increased Aliasing Frequency," in *Proc. of 124th Aud. Eng. Soc. Conv.*, (Amsterdam, The Netherlands), 2008.
- [2] J. Hannemann and K. D. Donohue, "Virtual Sound Source Rendering Using a Multipole-Expansion and Method-of-Moments Approach," *J. Aud. Eng. Soc.*, vol. 56, no. 6, pp. 473–481, 2008.
- [3] Y. J. Wu and T. D. Abhayapala, "Spatial multizone soundfield reproduction," in *IEEE International Conference on Acoustics, Speech, and Signal Processing (ICASSP)*, (Taipei, Taiwan), pp. 93–96, Apr. 2009.
- [4] S. Spors, K. Helwani, and J. Ahrens, "Local sound field synthesis by virtual acoustic scattering and time-reversal," in *Proc. of 131st Aud. Eng. Soc. Conv.*, (New York, USA), 2011.
- [5] S. Spors and J. Ahrens, "Local Sound Field Synthesis by Virtual Secondary Sources," in *Proc. of 40th Intl. Aud. Eng. Soc. Conf. on Spatial Audio*, (Tokyo, Japan), 2010.
- [6] E. G. Williams, *Fourier Acoustics: Sound Radiation and Nearfield Acoustical Holography*. London: Academic Press, 1999.
- [7] F. Zotter and S. Spors, "Is sound field control determined at all frequencies? How is it related to numerical acoustics?," in *Proc. of 52nd Intl. Aud. Eng. Soc. Conf. on Sound Field Control - Engineering and Perception*, (Guildford, UK), Sept. 2013.
- [8] S. Yon, M. Tanter, and M. Fink, "Sound focusing in rooms: The time-reversal approach," *J. Acoust. Soc. Am.*, vol. 113, no. 3, 2003.
- [9] D. de Vries and A. J. Berkhout, "Wave theoretical approach to acoustic focusing," *J. Acoust. Soc. Am.*, vol. 70, no. 3, 1981.
- [10] M. Fink, "Time reversal of ultrasonic fields. {I.} Basic principles," *Ultrasonics, Ferroelectrics, and Frequency Control, IEEE Transactions on*, vol. 39, no. 5, pp. 555–566, 1992.
- [11] E. Verheijen, *Sound Reproduction by Wave Field Synthesis*. PhD thesis, Delft University of Technology, 1997.
- [12] J. R. Shewell and E. Wolf, "Inverse Diffraction and a New Reciprocity Theorem," *J. Opt. Soc. Am.*, vol. 58, no. 12, pp. 1596–1603, 1968.
- [13] S. Spors and J. Ahrens, "Spatial Sampling Artifacts of Wave Field Synthesis for the Reproduction of Virtual Point Sources," in *Proc. of 126th Aud. Eng. Soc. Conv.*, (Munich, Germany), 2009.
- [14] S. Spors, H. Wierstorf, M. Geier, and J. Ahrens, "Physical and Perceptual Properties of Focused Sources in Wave Field Synthesis," in *Proc. of 127th Aud. Eng. Soc. Conv.*, (New York, USA), 2009.
- [15] E. W. Start, *Direct Sound Enhancement by Wave Field Synthesis*. PhD thesis, Delft University of Technology, 1997.
- [16] S. Spors and J. Ahrens, "Spatial Sampling Artifacts of Focused Sources in Wave Field Synthesis," in *NAG-DAGA International Conference on Acoustics*, (Rotterdam, The Netherlands), 2009.
- [17] B. Girod, A. Stenger, and R. Rabenstein, *Signals and Systems*. Wiley, 2001.
- [18] H. Wierstorf and S. Spors, "Sound Field Synthesis Toolbox," in *Proc. of 132nd Aud. Eng. Soc. Conv.*, (Budapest, Hungary), Apr. 2012.
- [19] H. Wierstorf, C. Hohnerlein, S. Spors, and A. Raake, "Coloration in Wave Field Synthesis," in *Proc. of 55th Intl. Aud. Eng. Soc. Conf. on Spatial Audio*, (Helsinki, Finland), Aug. 2014.